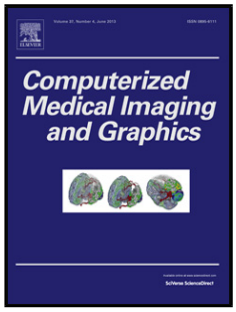

Title: A Computer-Aided Detection of the Architectural Distortion in Digital Mammograms using the Fractal Dimension Measurements of BEMD

Author: Imad Zyout Roberto Togneri

PII: S0895-6111(18)30185-X
DOI: https://doi.org/doi:10.1016/j.compmedimag.2018.04.001
Reference: CMIG 1557

To appear in: *Computerized Medical Imaging and Graphics*

Received date: 8-4-2017
Revised date: 1-4-2018
Accepted date: 2-4-2018

Please cite this article as: Imad Zyout, Roberto Togneri, A Computer-Aided Detection of the Architectural Distortion in Digital Mammograms using the Fractal Dimension Measurements of BEMD, *<![CDATA[Computerized Medical Imaging and Graphics]]>* (2018), https://doi.org/10.1016/j.compmedimag.2018.04.001

A Computer-Aided Detection of the Architectural Distortion in Digital Mammograms using the Fractal Dimension Measurements of BEMD

Imad Zyout[a,*], Roberto Togneri[b]

[a] *Communications, Electronics and Computer Engineering Department*
Tafila Technical University, Tafila, 66110, Jordan
[b] *School of Electrical, Electronic and Computer Engineering*
The University of Western Australia
35 Stirling Highway, CRAWELY WA 6009 Australia

Abstract

Achieving a high performance for the detection and characterization of architectural distortion in screening mammograms is important for an efficient breast cancer early detection. Viewing a mammogram image as a rough surface that can be described using the fractal theory is a well-recognized approach. This paper presents a new fractal-based computer-aided detection(CAD) algorithm for characterizing various breast tissues in screening mammograms with a particular focus on distinguishing between architectural distortion and normal breast parenchyma. The proposed approach is based on two underlying assumptions: i) monitoring the variation pattern of fractal dimension, with the changes of the image resolution, is a useful tool to distinguish textural patterns of breast tissue ii) the bidimensional empirical mode decomposition (BEMD) algorithm appropriately generates a multiresolution representation of the mammogram. The proposed CAD has been tested using different validation datasets of mammographic regions of interest (ROIs) extracted from the Digital Database for Screening Mammography (DDSM) database. The validation ROI datasets contain architectural distortion(AD), normal breast tissue, and AD surrounding tissue. The highest classification performance, in terms of area under the receiver operating characteristic curve, of $Az = 0.95$ was achieved when the proposed approach applied to distinguish 187 architectural distortion depicting regions from 2191 normal breast parenchyma regions. The obtained results validate the underlying hypothesis and demonstrate that effectiveness of capturing the variation of the fractal dimension measurements within an appropriate multiscale representation of the digital mammogram. Results also reveal that this tool has the potential of prescreening other key and common mammographic signs of early breast cancer.

Keywords: Mammography, Computer-Aided Detection, Architectural Distortion, Bidimensional Empirical Mode Decomposition, Fractal Dimension

1. Introduction

Breast cancer is the most common cancer that kills women around the world. Statistics from 2011 indicated that in the United States (US) 1 in 8 women is at risk of developing invasive breast cancer in her life time. In the European Union (EU), breast cancer accounts for 1 in every 6 female deaths from cancer [1]. The detection and diagnosis of the disease in its early stages has been shown to be very important toward better breast cancer survival rates. Mammography, an X-ray based breast imaging modality, is currently the most effective tool for screening and for detecting the disease in its infancy when it is more curable. Early signs of breast cancer commonly considered by radiologists during mammography reading are: calcifications, masses, architectural distortion, and bilateral asymmetry[2]. The double reading of screen mammograms has been shown to reduce the number of missed cancers. However, securing such a process is mostly not feasible and not cost effective. Over the years researchers have made extensive efforts to develop computer aided detection and diagnosis (CAD) systems that can provide radiologists with a second opinion and as an alternative to the double reading[3]. Among the most common early sign

*Corresponding author
Email addresses: izyout@ttu.edu.jo (Imad Zyout), roberto.togneri@uwa.edu.au (Roberto Togneri)

of nonpalpable breast cancer detected mammographically, the prevalence of architectural distortion is low and ranked third after calcifications and masses. However, architectural distortions subtlety and obscured nature, and variable appearance make the detection task more difficult and challenging[5]. Moreover, retrospective analysis of false negative results has shown that about 12% to 45% of misinterpreted screening mammograms turned out to be architectural distortion findings [6]. For this, early and accurate detection of architectural distortion potentially can improve the breast cancer prognosis. Compared to masses and calcifications, the performance provided by existing architectural distortion CAD algorithms has not yet reached satisfactory levels and hence more research focus is needed.

In the past decade, several approaches have been developed for the detection of architectural distortion. In [7], the application of image morphology and concentration index methods,respectively, produced sensitivity rates of 94% with 2.3 false positives per image and 84% with 2.4 false positives per image. Fractal analysis was used in [8],[9],[10] to distinguish between normal breast tissue and architectural distortion in mammographic regions. The application of the Gabor filter and phase portrait analysis was used in[11],[10]. Multiscale analysis and linear structure characterizing was employed by[12]. The use of spicularity and angular dispersion measures was investigated by [13]. The biggest coefficients from curvelet transform were also used as textural features to classify various mammographic abnormalities (including architectural distortions) contained in the MIAS database [14]. Other studies[15] and [16] proposed a unified approach to detect both spiculated masses and architectural distortions by considering the speculated patterns as a common feature between the two abnormalities. Sampat et al. [16] applied radial spiculation filters to enhanced images. For a dataset of 45 images, with architectural distortion images a sensitivity of 80% at 144 false positives per image was obtained.

Viewing the intensity of medical images including mammography as rough surfaces that can be described using the fractal theory has been recognized by many studies[20],[8]. The fractal dimension(FD) is a useful tool for characterizing the variation of structure details (or image features) as measuring scale changes [17] and for measuring the roughness of an image surface [19]. For mammography, it is known that normal breast parenchyma demonstrates a strong self similarity and so the fractal behavior can be observed to some extent. The fractal based assessment of mammographic prenchymal of the breast indicated a better match to a human expert's evaluation than the conventional procedure [20]. The presence of different breast abnormalities such as architectural distortions and masses was found to alter the fractal properties of normal breast tissue, which have been utilized in [8],[9] to characterize and to detect breast cancer. For the detection of architectural distortions, in particular, the statistical analysis [8] indicated the mammographic regions with AD exhibiting an average fractal dimension that is lower than that of the regions with normal breast tissue. Tourassi et al.[8] used the fractal dimension to discriminate between breast regions depicting architectural distortion and normal breast tissue. The fractal dimension was estimated using the circular average power spectrum technique and used as a decision variable to construct the receiver operating characteristics(ROC) curve. Using a dataset with 1388 regions representing normal breast tissue and 112 abnormal regions depicting architectural distortion extracted from the DDSM database, the obtained performance, measured in terms of the area under ROC curve (AUC) or Az value, was 0.89.

Rangayyan et al.[10], first, applied Gabor filters and phase portrait analysis to perform node analysis of mammogram images and to detect specious regions of architectural distortion, then, they used the fractal dimension, computed using the average circular power spectrum, and Haralick textural descriptors to reduce the number of false positive results by classifying specious regions into abnormal (with architectural distortion) regions and normal ones. The proposed approach was tested on prior and detection mammograms from which, respectively, 21 and 18 architectural distortions and 365 and 380 normal regions were obtained. A prior mammogram is the mammogram acquired before the detection of cancer [3] while the detection mammogram is the mammogram on which the cancer is identified. Using the fractal dimension alone, they achieved a classification performance in terms of Az value of 0.68 on datasets from detecting mammograms and 0.74 on the dataset from prior mammograms. The performance, on the prior mammogram regions, was further improved to $Az = 0.80$ using the fractal dimension, three Haralick textural descriptors and a Bayesian classifier.

Tourassi et al. used fractal dimension to characterize the presence of architectural distortion in mammographic ROIs. On a dataset of 1500 ROIs of which 112 depicting architectural distortion and 1388 related to normal breast tissue, an ROC with Az of 0.89 was obtained. Guo et al.[9] applied the lacunarity and fractal(another fractal property) to improve the fractal-based detection of the architectural distortions. On a ROI dataset with 19 architectural distortion and 41 nor-

mal regions, applying lacunarity and the fractal dimension (estimated using the fractional Brownian motion method) features with an SVM classifier, achieved an area under ROC curve of 0.875 .

In estimating the fractal dimension of digital images, in theory, the measured fractal dimension must not be affected by the pixel size (or the image resolution). In fact, this was found to hold for some pixel resolutions but varying the pixel size beyond some level (or size) has been shown to affect the estimated fractal dimension [21]. Ahammer et al. [21] observed that the pattern in which the estimated fractal dimension varies with image resolution (or pixel size) changes was different for different fractals and such variation itself can be employed as a tool for textural-based classification of images. For screening mammograms, measured fractal dimension was also found to vary with the image resolution. Tourassi et al. [8] related experimental work demonstrated that the performance of fractal dimension for discriminating between normal and abnormal mammographic regions had influenced by the pixels size with the down-sampling used to change the scale or the pixel size and concluded that monitoring fractal properties of mammographic images over different scales might be a useful tool for prescreening architectural distortions. It is worth noting that in [8] the variation of fractal dimension measurements with scales was only observed but not used for the detection of architectural distortion.

Consequently, key contributions of this study are: capturing the variation and fractal dimension measurements over multiscale representation and its application for architectural distortion prescreening and detection. Another and second contribution is the use of the 2D EMD for generating multiscale representation of mammographic images. The underlying hypothesis of this paper is that, for the fractal-based characterization of breast tissue, capturing the variation of the fractal dimension measurements with the change of the image resolution (or pixel size) has the potential to differentiate between architectural distortion and normal breast tissue. For this purpose, the bidimensional empirical mode decomposition (BEMD) [22] and filtering algorithm [23], an alternative to the simple the image subsampling process, is first employed to produce the multiresolution representation of an image. Fractal dimension measurements are, consequently, estimated from the multiscale representation and used for the classification of normal and abnormal breast tissue.

The empirical mode decomposition (EMD) algorithm was first introduced by Huang et al. [22] as an adaptive and data driven multiresolutional decomposition and filtering algorithm that suits various signals. The basic concept of the EMD approach is to decompose the original signal into a complete and almost orthogonal set of components namely intrinsic mode functions (IMF) and a residue. The extension of the one-dimensional EMD algorithm [22] to process digital images, called the bidiminsional EMD (BEMD), was proposed by Nunes et al.[23]. Further and several refinements and modification to the two-dimensional EMD were also proposed by [24] and [25]. Among these modifications the fast and adaptive BEMD (FABEMD) [25] is the most interesting since it facilitates applying BEMD to large-size images such as mammograms without significantly jeopardizing the essential properties of the BEMD by providing an alternative and efficient method for accomplishing the envelope estimation process. Since EMD and BEMD algorithms were introduced, several studies have applied BEMD algorithms for the pattern analysis of computer-aided detection of breast cancer [27] [28], [29], [35]. Caroline et al. [35] applied ensemble EMD with adaptive noise and GLCM feature extraction methods for the detection and diagnosis of masses in mammographic regions obtained from the MIAS database. Authors [35] also suggested,as a future work, the extraction of fractal dimension of IMF components to improve the proposed algorithms. For the detection of architectural distortion,particularly, previous studies [28] applied BEMD and statistical modeling of detail subbands (i.e. 2DIMF) to distinguish architectural distortion depicting ROIs from normal breast tissue. On a ROI dataset of 187 and 887 normal regions, the classification performance A_z of 0.88 was produced. Also, the generalized Gaussian models of BEMD and the fractal dimension(estimated from original image rather than it's BEMD), were also used to characterize the architectural distortion surrounding tissue [29]. Results of this work revealed that the textural patterns of surrounding tissue are statically different form normal breast tissue. On a set of 353 surrounding tissues (extracted from abnormal or architectural distortion mammograms)and 2191 normal ROIs, the best architectural distortion recognition performance achieved was A_z of 0.869.

In this paper, we propose to apply multiscale fractal dimension measurements for characterizing different textures of breast tissue, with focus on the architectural distortion detection in screening mammograms, as follows: the BEMD image approach, is first applied for generating adaptive and data driven multiresolutional decomposition of the mammogram image. Then, the fractal dimension is estimated from each resolution and used for distinguishing between normal and abnormal

regions. The feature vector formed, from the multiscale fractal dimension measurements, is subsequently used for the classification of different texture of breast tissue. To the best of our knowledge this study is the first to propose to apply fractal based analysis of BEMD image decomposition for characterizing and classifying architectural distortion and normal breast parenchyma.

2. Materials and Methods

2.1. Overview of BEMD

Different versions of the EMD approach commonly accomplish the multiscale decomposition of the original signal using three basic steps: 1) the extraction of minima and maxima 2) estimation of the lower and upper envelopes corresponding to the minima and maxima maps, respectively, and 3) formation of the mean envelope to produce an IMF from the original signal. However, accomplishing lower and upper envelope estimation using cubic spline or radial basis function methods is computationally expensive and is a major challenge facing the application of the BEMD to analyze images of large size. To address this problem, several modifications have been introduced [25], [24],and [30]. The BEMD algorithm applies a sifting process [22] to decompose a discrete time signal $f(x, y)$ into a set of two-dimensional intrinsic mode functions (IMFs), $imf_i(x, y)$ $i = 1, 2 \ldots, N$ and a residue signal, $r_N(x, y)$:

$$f(x, y) = \sum_{i=1}^{N} imf_i(x, y) + r_N(x, y), \quad (1)$$

The sifting process [22] was mainly proposed to refine the extraction of the IMF components such that each IMF meets the following two requirements:

- The total number of extrema (minima and maxima) and the number of zero-crossings must equal or differ at most by one.
- The mean value of the upper and lower envelopes, at any point, is equal to zero.

Indeed, the IMF and residue components (images or 2D signals) from (1), can be seen to be equivalent but not equal, to the details and approximate subbands (images) produced by wavelet or filter bank approaches[37].

We define a source signal (or image), $f(x, y)$,as being eligible for BEMD calculation if it has a sufficient number of extrema, at least two; one maximum and one minimum [22]. The process of extracting the intrinsic modes of the signal, namely the IMF and the residue components using the BEMD algorithm is described as follows

- Initialize the IMF index, $i = 1$, and let the residue signal $r_{i-1}(x, y) = f(x, y)$.
- Define the sifting process stopping criteria, which are the maximum number of iterations allowed, J, and SD_{max} the limit on the standard deviation between two successive results of the sifting process.
- Initialize the iteration index $j = 1$ and the source image $h_{j-1}(x, y) = r_{i-1}(x, y)$
- Extract the *ith* IMF (i.e. $imf_i(x, y)$ or IMF_i) by applying the sifting process to the source image $h_{j-1}(x, y)$

While { j ≤ J

1. Identify the local minima and maxima in $h_{j-1}(x, y)$
2. Estimate the lower $E_{Lower}(x, y)$ and upper $E_{Upper}(x, y)$ envelopes from the minima and maxima maps, respectively.
3. Compute the envelopes mean, $M_{j-1}(x, y) = (E_{Lower}(x, y) + E_{Upper}(x, y))/2$
4. Compute $h_j(x, y) = h_{j-1}(x, y) - M_{j-1}(x, y)$
5. Compute the standard deviation between $h_{j-1}(x, y)$ and $h_j(x, y)$

$$SD = \frac{\sum_{x=1}^{N_x} \sum_{y=1}^{N_y} |h_j(x,y) - h_{j-1}(x,y)|^2}{\sum_{x=1}^{N_x} \sum_{y=1}^{N_y} |h_{j-1}(x,y)|^2} \quad (2)$$

6. Check if the first stopping criterion is met
   If $SD \leq \mathrm{SD}_{max}$
   - Obtain the IMF and residue components
     $imf_i(x, y) = h_j(x, y)$
     $\mathrm{r}_i(x, y) = r_{i-1}(x, y) - imf_i(x, y)$
   - Break the current loop (i.e. terminate the sifting process)

   Else
   - Increase the iteration index $j = j + 1$ (i.e. apply sifting steps again)

   End

- If the obtained residue $r_i(x, y)$ is eligible for BEMD, increase the IMF component index $i = i+1$ and re-apply the sifting process to extract a new IMF. Otherwise, the BEMD algorithm is terminated.

As previously mentioned, this study derives the BEMD of mammographic regions using the FABEMD [25] version of BEMD algorithms [23] and [26]. The main difference between the standard BEMD [23] and

FABEMD is in the method used for performing the estimate of the lower and upper envelope that is a key step for BEMD. Using the FABEMD method, the envelop estimation is done by applying a 2D order statistics filtering instead of the use of classical scattered data surface interpolation technique [26].

The envelop estimation process using the FABEMD [25] approach is accomplished by two steps as follows:

- The determination of the filter size (2D sliding neighbourhood or window) is done by constructing arrays correspond to the smallest Euclidian distance between each minimum (maximum) and other minima(maxima). From these arrays, the sizes of the order-statistics filters can be obtained.
- The estimation of the lower and upper envelops is done by applying minimum and maximum filtering to the sliding neighborhood of $h_{j-1}(x, y)$, to construct the lower $E_{Lower}(x, y)$ and upper envelope $E_{Upper}(x, y)$, respectively. Using the same window size as used for minimum and maximum filtering, another sliding window smoothing filter is then applied to further improve the estimated lower and upper envelopes.

The FABEMD provides different filter or window lengths (or sizes) for performing the BEMD of the original signal. However, one can still perfectly, within machine precision error, recover the original signal from any of its BEMDs (or multiscale representations). As indicated in [25] the previous method for determining the size of the filter may require manipulation if both window sizes obtained for the new scale are both smaller than the previous one. However, one should avoid high degree of time-sale (or filter size) manipulation so the time-driven feature of the original EMD is lost.

2.2. Fractal Dimension

For the analysis of image texture, it was observed that the human observer's subjective ranking and the fractal dimension are strongly correlated [20]. The basic concept of the fractal dimension measurements is to measure an image feature (energy, intensity difference, edges) as a function of the scale. If the variation of the feature to the scale changes is plotted on a log-log plot, a linear relation is obtained where the fractal dimension is linearly related to slope of that relation. Several methods were developed for estimating the fractal dimension of grayscale images [18]. A popular and efficient method for estimating the fractal dimension is based on fractional Brownian motion model (FBMM) to describe rough surfaces that are seen as the end result of a random walk. Intensity medical images and ultrasonic and x-ray images can be similarly viewed and has enabled the use of the FBMM to estimate the fractal dimension of medical images [19]. For mammography, in particular, the FBMM method has been shown to be the most efficient over other methods[9].

Given an image region $f(x, y)$, of size $N_x \times N_y$, a useful measure of the roughness of the image surface, the fractal dimension D, can be computed from the following equation:

$$gd(s) = us^H \tag{3}$$

where u is a constant, s is the scale (distance in pixels) variable and $gd(s)$ is the expectation of the intensity variation of the pixels separated by a distance s:

$$\begin{aligned} gd(s) = \frac{1}{2N_x(N_y-s)}(\sum_{x=1}^{N_x}\sum_{y=1}^{N_y-s}|f(x,y)-f(x,y+s)| \\ +\sum_{x=1}^{N_x-s}\sum_{y=1}^{N_y}|f(x,y)-f(x+s,y)|) \end{aligned} \tag{4}$$

The H parameter, which characterizes the image surface, is to be estimated and is related to the fractal dimension D using the equation $H = 3 - D$. Computing the log of (3) gives:

$$\log gd(s) = \log u + H \log s \tag{5}$$

The least square linear regression is used,then, to estimate the slope H of the line equation, on a log-log scale to obtain the fractal dimension as:

$$D = 3 - H \tag{6}$$

2.3. Mammogram datasets

Mammographic regions of interest (ROIs) will be used for evaluating the proposed mammography CAD and architectural distortion characterization approach are obtained from the DDSM databse [31]. Another mammography databases commonly used for evaluating mammography CAD algorithms is the Mammographic Image Analysis Society (MIAS) [32] database. However, the MIAS database compared to DDSM is relatively small and only includes 322 digitized mammograms with 8 bits per pixel, 200μm pixel resolution, and sized 1024×1024. For this, the application to MIAS dataset will be only for the comparison with other studies. The DDSM database, on the other hand, is much larger with screening mammograms digitized at three different pixel resolutions (42,43.5, and 50μm) and two different bit depths (12 and 16 bit per pixel). Radiologists' annotations of abnormal DDSM cases included

in an *.ics* file accompanied each case also reports the patients age, at the time of the data acquisition, and abnormality description according the Breast Imaging Reporting and Data System (BI-RADS) lexicons [4].

This work used three different validations ROI datasets extracted from abnormal and normal DDSM mammograms. The datasets, shown by Table 1, represent architectural distortion or true positive (TP) regions, normal breast parenchyma or true negative (TN) regions, and AD surrounding tissue (ST) regions. The TP and AD depicting ROI dataset consists of 187 architectural distortions extracted from 187 abnormal mammograms. The normal dataset consists of 2191 TN regions obtained from 261 mammograms (about 8 regions per mammogram) from DDSM normal volumes produced by LUMISYS and HOWTEK mammogram digitizers. The surrounding tissue ROI dataset consists of 558 regions extracted from 187 abnormal mammograms (images already used to obtain AD regions). The size of AD depicting ROI is proportional to the lesion size and varies from one case to another. Selecting the size of a normal regions, to some extent, is open, however, computing BEMD and estimating the fractal dimension have been also taken into consideration. Hence, in this work, normal ROIs allowed to have two sizes 512×512 or 384×384 pixels. These adopted sizes were around the mean size of abnormal samples but also considering the normal mammogram from which TN samples were extracted. The application to MIAS database, in this work, was mainly to compare with existing studies. The MIAS contains 115 abnormal cases from which only 19 cases are with architectural distortion are used as TP dataset, and 207 normal cases from which a set 41 mammograms were used to obtain the TN regions. Examples of abnormal and normal ROIs extracted from the DDSM database are shown in Fig. 1. To display the outline and location of AD in the region,in Fig. 1, the size of the abnormal region used were larger than the actual size used for the analysis.

The surrounding tissue dataset were obtained from the same abnormal images previously used to extract TP or AD regions. That is subsequent to localizing the rectangle ROI including the AD (using the mammogram annotation provided by the DDSM), eight neighboring regions were extracted and considered potential surrounding tissue regions. However, in a semi-supervised approach, candidates surrounding tissue were checked and those regions overlap with pectoral muscle or background were eliminated. The size of ST regions was originally the same as size that of AD region, however, to avoid elimination of most ST regions, regions were then cropped to 512×512 or 384×384 pixels. Using this process a surrounding tissue (ST) dataset with 558 regions were obtained. Furthermore, important factors impacting the task of mammographres are mainly the density of the breast (in both normal and abnormal mammogram),and the subtlety (or visibility) of the lesion and its severity. The distribution of breast densities of abnormal and normal mammograms images, used in this work, are presented in Fig. 2. For abnormal mammograms used, the distribution of lesion's subtlety and severity are shown in Fig. 2(b).

Table 1: The distribution of different breast tissue regions in each ROI dataset

Database	Dataset	# AD	# TN	#ST	Region size(in pixels)
DDSM	S_1	187	2191	–	384×384, 512×512
	S_2	187	–	558	384×384, 512×512
	S_3	–	2191	558	384×384, 512×512
MIAS*	S_4	19	41	–	128×128

* The MIAS ROI dataset is mainly used for comprasion with other studies

3. Mammography CAD using the Fractal Dimension Measurements of BEMD

To investigate the usefulness of image representation using BEMD for the fractal based characterization of architectural distortion, we apply the proposed methods to distinguish between abnormal mammographic regions depicting architectural distortions in the center and normal regions representing normal breast parenchyma. The proposed mammographic regions (or images) and architectural distortion CAD system, first applies the FABEMD method to accomplish an adaptive and data driven multiscale decomposition, namely the IMF components of the original mammographic image, then, the fractal dimension estimated using FBMM is computed for each IMF to obtain a textural feature vector for classification. The well-known nonlinear SVM classifier with radial basis kernel function is employed to distinguish between patterns of normal and abnormal regions.

Mammographic Region Extraction: in this stage, the abnormal mammographic regions are extracted using the lesion annotations provided by each database with the size of each rectangular region chosen to best fit the abnormality, while the normal regions are extracted from normal mammograms as in[9]where normal but suspicious regions to be included are restricted to have a fractal dimension value between 2.0 to 2.9.

Bidimensional empirical mode decomposition (BEMD): For decomposing mammographic images using BEMD, several experiments have been performed by varying the maximum iteration, sifting process stopping criterion, and filter size used for the envelope

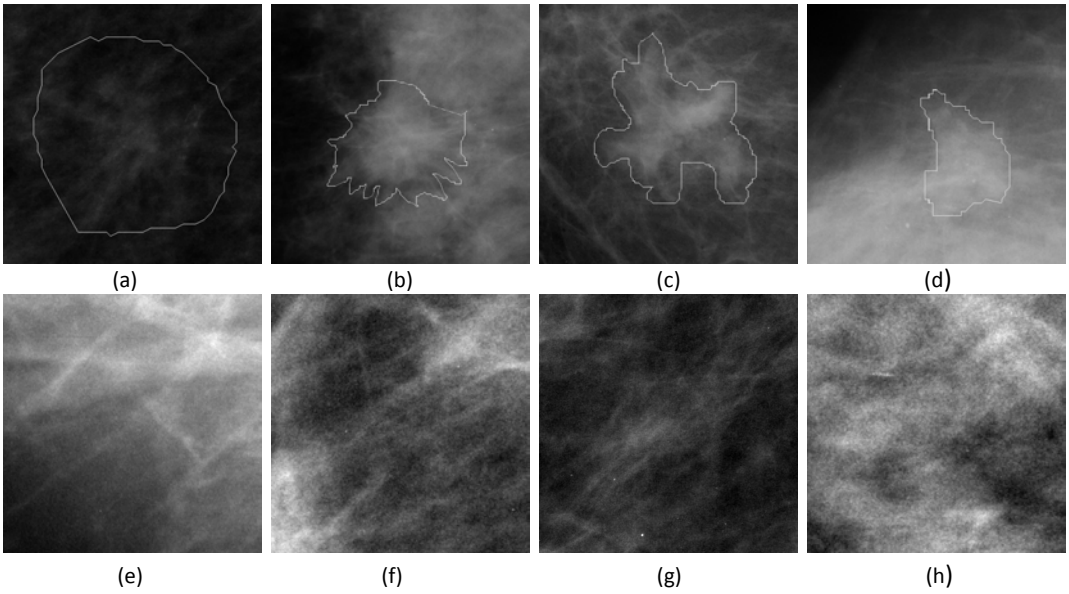

Figure 1: Examples of mammographic regions representing architectural distortion in (a) - (d) and normal breast parenchyma in (e)-(h). Architectural distortion related regions, shown in this figure, were obtained from the DDSM abnormal mammograms in the cancer volume 9 (a)case0230 (Right breast, MLO view) (b) case3390 (left breast, CC view) (c) case3407 (right breast, CC view) and (d) case3078 (Right breast, CC view).

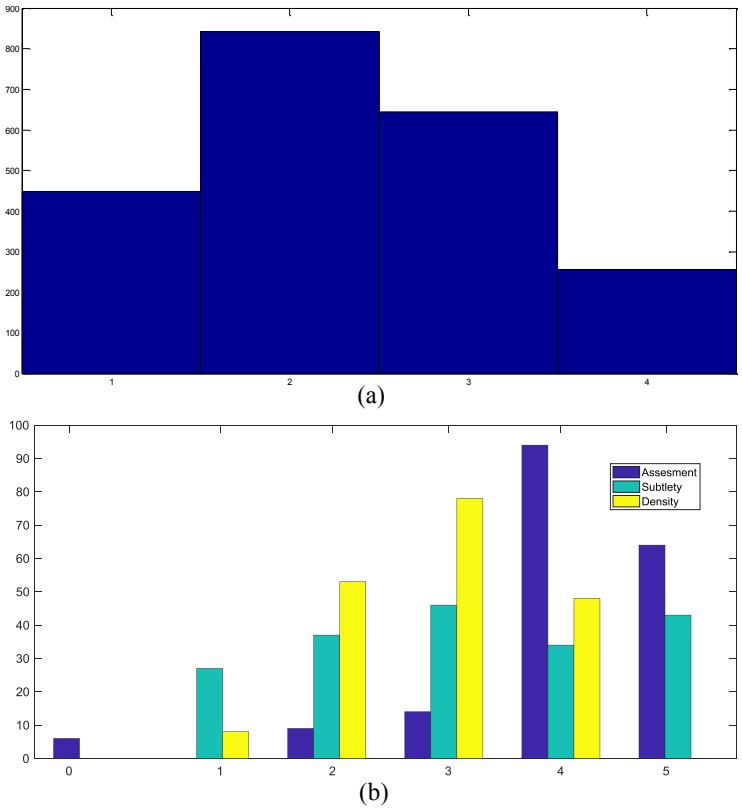

Figure 2: (a)Distributions of breast density, in scale of 1 to 4, in normal mammograms used.(b)Distributions of abnormalities in mammograms used, in terms of, the breast density, in scale of 1 to 4, the lesion Subtlety or visibility, in scale of 1(subtle) to 4 (obvious),and the ACR (BI-RAD) assessment rating of the lesion between 0 and 5.

estimation. We have empirically selected to use the IMF decomposition parameters with a maximum number of iterations of 4 and SD_{max} of 0.2 . For extending an image along the boundaries that is required for filtering signals (or images) with finite representation, the traditional symmetrical extension (or mirrorizing) technique is used [33].For an efficient EMD analysis, EMD research studies suggested that one needs to avoid the use of very low resolution (or undersampled) signals or apply a sifting process with a large number of iterations or very small SD_{max} values [36]. Unlike the case of the classical wavelet decomposition [37] where the maximum number of detail subbands (or scales) that can be attained mainly depends on the image size, for EMD decompositions, the maximum number of IMF components (or scales) produced from the original signal is data driven. Particularly using the MIAS dataset where mammogram images are only 8 bits per pixel and 200μ pixel size, most images produce BEMD decomposition with 5 IMFs while some images produce 6 IMFs. For DDSM mammographic regions, the situation is different and a higher number of IMFs are expected to be provided because DDSM mammograms are more detailed since the pixel depth is from 12 to 16 bits and the pixel resolution is between 42 and $50\mu m$. In this study, 5 and 6 IMFs will be used for the analysis of images from MIAS and DDSM datasets, respectively. Examples of the BEMD algorithm applied to abnormal and normal MIAS mammographic regions are shown in Figs. 3 and 4. To ensure that the pattern representation and so the number of features obtained is the same for all samples (or images), the number of IMF components that is common for all images, in our datasets, is used for feature extraction and for pattern classification.

Fractal Dimension Estimation: the FBMM fractal dimension method, used in this analysis, is adopted for its ability to estimate the fractal properties directly from the original image without further processing. Moreover, it has been shown to be superior over other methods, in particular, FBMM was proven more efficient than the conventional power spectrum technique for fractal analysis of mammograms [9]. The FBMM, as explained in Section 2, was applied to the IMF components obtained from the BEMD. This step produces feature vectors representing the fractal dimension measurements of each mammographic region as

$$D = [D_0, D_1, D_2, ..., D_N] \quad (7)$$

where N is the maximum number of IMF components D_0 denotes the fractal dimension of the original image while D_i, for $i = 1, 2 \ldots, N$, represents the fractal dimension of the *ith* IMF component. An example of the fractal dimension measurements obtained from BEMD analysis of an abnormal region is illustrated in Fig. 5.

Pattern recognition using SVM classifier: over the years, SVM classifiers have demonstrated superior performance for solving different machine learning problems including the development of mammography CAD systems [2]. The properties of an SVM based pattern classification that suits different pattern recognition problems are 1) the ability to be trained using a small number of samples 2) able to work with both high dimensional and low dimensional feature spaces 3) can be applied to solve both one-class, binary or two-class, and multi-class problems. The machine learning approach of the SVM classification is derived from modern statistical learning theory. An SVM classifier finds an optimal hyper-plane that maximizes the separation (geometric margin) among the patterns from different classes [38]. Further details on SVM theory can be found in [38] and [39].

4. Results

4.1. Experimental setup

In the SVM classification stage, the libsvm software package [40], MATLAB interface, with the nonlinear SVM and radial basis function kernel options, has been used. A grid search with C value between 0.5 and 1048576 and kernel control parameter γ value between 0.0625 and 16 were, respectively, employed for the SVM penalty (or regularization) constant and for the Gaussian kernel control parameter. For the performance evaluation, each datasets is partitioned into 50% training and 50% testing. A 5-fold cross validation procedure and grid search procedure were applied to the training dataset to optimize the classification performance.

Using the BEMD approach presented in Sections 2 and 3 , six IMF components were produced by mammographic regions from DDSM datasets.On the other hand, the low pixel resolution regions from the of MIAS database provide only five IMF layers per region. In order to evaluate the contribution of various IMF components, the fractal dimension features of the IMF components are successively included for the classification and the obtained performance has been evaluated and reported. Moreover, we have examined the impact of including the fractal dimension of the original image with the fractal measurements from all IMFs in one experiment and with the first IMF only in another experiment.

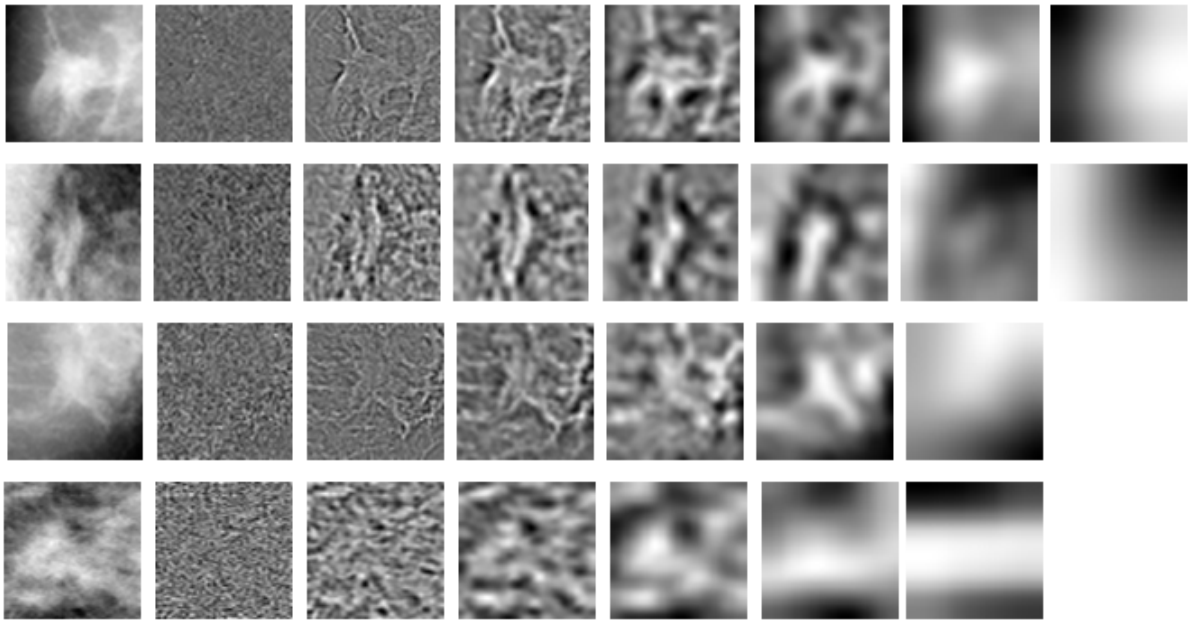

Figure 3: Applications of BEDM algorithm to mammographic regions depicting architectural distortion. In each row, the original image is placed first, followed by extracted IMFs components (or images) and the residue component is the last subimage

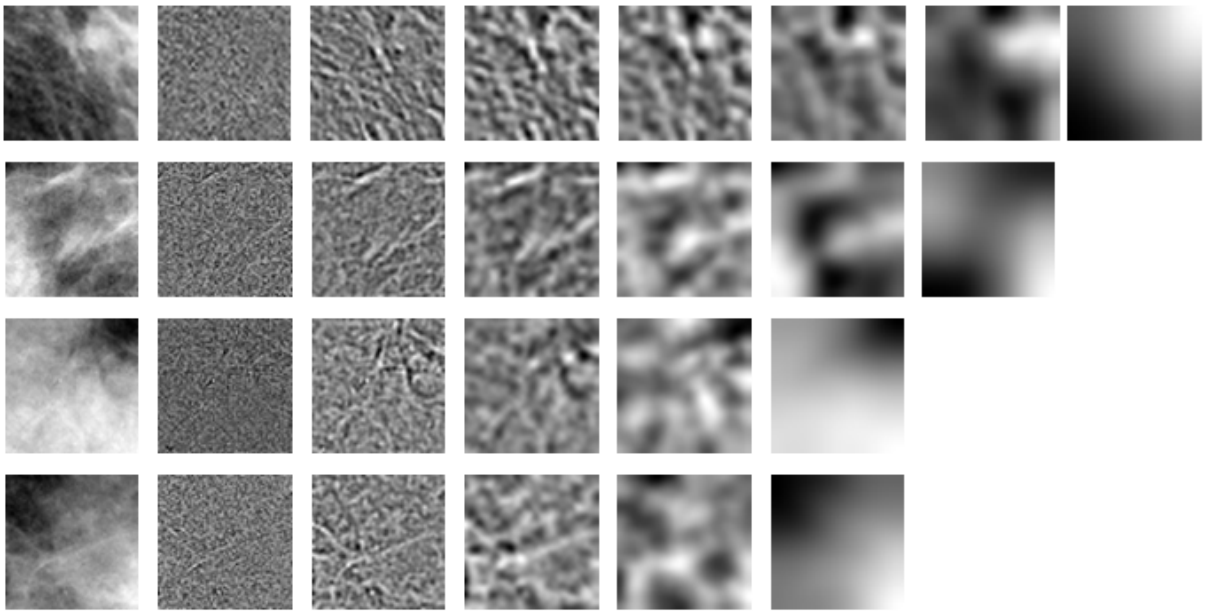

Figure 4: Applications of BEDM algorithm to mammographic regions related to normal breast tissue. In each row,again, the original image is placed first, followed by extracted IMFs components (or images) and the residue component is the last subimage.

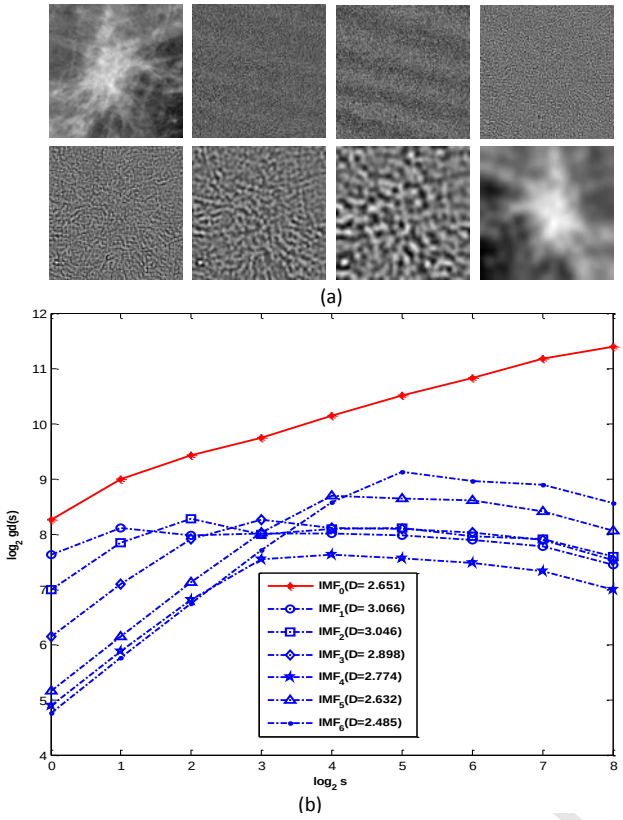

Figure 5: BEMD and fractal dimension measurements applied to an architectural distortion region from the DDSM dataset (case1140, cancer volume 6). (a) An AD image and its BEMD; the original image is placed first, followed by its IMF and residue components.(b) The FBMM technique applied to estimate the fractal dimension of the original image and its BEMD with the expectation of the intensity variation $gd(s)$, plotted on the log-log scale, against the scale s (i.e.the separation-distance in pixels). The fractal dimension of each image is,then, computed from the linear fit of the corresponding log-log plot.

4.2. Analysis of fractal dimension measurements

After extracting intrinsic components (i.e. 2D IMF layers) of each mammographic region, the fractal dimension is estimated, as explained in Section 3, from each image (original or IMF) using the FBMM technique. A feature vector representing each mammographic region is constructed, as previously discussed, to be used subsequently for the classification between abnormal and normal regions. Previous analysis [8], [10], [9] of fractal properties of AD and normal breast parenchyma has indicated that presence of an architectural distortion disturbed the fractal properties of normal breast parenchyma and so a lower fractal dimension of mammographic regions was observed, which was used as tool for architectural distortion prediction. In this work, measurements shown in Table 2, have also demonstrated that the average FD estimated for AD regions (original image) is lower than that of TN regions. This observation is also observed for FD measurements from IMF components. That is the average fractal dimension of BEMD (including detail and residue layers) of abnormal or AD depicting regions was lower than the corresponding values from normal regions. This observation also extends for ST regions that demonstrate average FD that is lower than TN regions but higher than AD regions. For instance, respectively for normal, abnormal or AD, ST regions the fractal dimension estimated from IMF_0 (i.e. original region) were 2.707 ± 0.104, 2.575 ± 0.071 and 2.678 ± 0.107.

Table 2: Average fractal dimension measurements of BEMD (i.e. 2DIMF layers) for different breast tissue types

IMF layer	TN	AD or TP	ST
D_0	2.707 ± 0.104	2.575 ± 0.071	2.678 ± 0.107
D_1	3.064 ± 0.01	3.053 ± 0.014	3.057 ± 0.014
D_2	3.059 ± 0.01	3.051 ± 0.024	3.071 ± 0.029
D_3	2.905 ± 0.042	2.888 ± 0.067	2.895 ± 0.043
D_4	2.775 ± 0.049	2.744 ± 0.058	2.765 ± 0.053
D_5	2.649 ± 0.062	2.619 ± 0.072	2.634 ± 0.066
D_6	2.523 ± 0.073	2.493 ± 0.09	2.504 ± 0.078

4.3. Statistical analysis

The average FD estimated from various IMF layers, as shown by results in Table 2, is different among three classes of breast tissue (i.e. AD, normal parenchyma, and ST tissue). To examine whether the difference of FD value among different breast tissue is statically significant, so, it can used for the detection of AD, we have used the two tail *t-test* of the null hypothesis (H0: equal mean). The *t-test* was applied to examine the statistical significant of the discrimination, based on the FD, between AD tissue and normal breast parenchyma (AD vs TN), in one experiment, and the discrimination, in another experiment, between normal breast parenchyma and surrounding tissue (ST vs TN). Also for classifying AD from surrounding tissue (AD vs ST). For distinguishing between AD and normal breast tissue, the differences of FD measurements from all layers were statically significant. That is attained *p-value* and the 95% confidence interval (CI) suggest rejecting the null hypothesis (i.e. the two mean are equal), as none of the corresponding 95% CI contains 0. As shown by test resutls in Table 3 The difference of FD between normal breast parenchyma and surrounding tissue were also

statically significant but not for all FD measurements, namely, FD of the first IMF layer that produced *p-value* of 0.7693 that is larger than 0.05. The staticial anslysis of FD measurments' difference between srrounding tissue and AD regions indicated that the difference of FD measurments of low-frequency layers (D_4,D_5, and D_6) is not signficant. Hence, the use of FD features of the fourth, fifth, and sixth layers is expected to be not efficient for classification. Results of the statistical analysis of the difference of the FD measurements over BEMD scales reveal the potential of the FD for distinguishing between AD and normal breast parenchyma.

Table 3: Statistical significance(*p-value*) of FD measurements for characterizing different classes of breast tissue

Feature	AD vs TN	ST vs TN	AD vs ST
D_0	≈ 0	0.0010	≈ 0
D_1	≈ 0	0.7693	≈ 0
D_2	≈ 0	≈ 0	≈ 0
D_3	0.0024	0	0.049
D_4	≈ 0	0	0.427
D_5	≈ 0	0	0.500
D_6	≈ 0	0	0.158

4.4. Pattern recognition results

The kernel based SVM classifier was used for pattern recognition of different breast tissue. The classification results obtained from different experiments are presented in Tables 4-6. The average cross-validation and test performance, in terms of *Az* value, form all runs, were reported and used for the evaluation. For the distinguishing between architectural distortion and normal breast parenchyma regions, the classification results, of FD features of BEMD are shown in Table 4. The best classification performance of 0.941 ± 0.009 was obtained using $D_3D_2D_1$ (derived from 3IMFs). Results also indicate that the use of all available IMF layers including the original image to accomplish the fractal dimension analysis has not provided any performance improvement. For instance, the fractal analysis, using $D_6D_5D_4D_3D_2D_1D_0$ and $D_6D_5D_4D_3D_2D_1D_0^\star$ respectively produced an average *Az* of 0.936 ± 0.009 and 0.882 ± 0.005. The poor performance achieved by more features can be justified by the weak discriminative power of the fractal measurements of IMF components corresponding to the lower image resolutions. In Fig. 6, the best ROC curve, corresponds to each features, was also produced and constructed. To answer the question whether the fractal properties of the surrounding tissue are relevant to architectural distortion or to normal breast parenchyma, we applied BEMD fractal dimension measurements to discriminate surrounding tissue from architectural distortion and from normal breast parenchyma regions. Obtained classification results, in Table 5, show that FD measurements of the first three IMF layers achieved the highest average A_Z of 0.854 ± 0.013. Results also showed that the inclusion of D_0 can be used to achieve higher A_Z value. Results also revealed that the contribution of FD measurements from low-frequency layers (i.e. D_4,D_5, and D_6) is almost negligible even might be deteriorating. Moreover, examining results of applying multiscale FD features to distinguish ST from normal breast tissue, in Table 6, the highest classification performance of 0.771 ± 0.007 was produced using FD features D_1D_2. This, however, is significantly lower than the performance of D_1D_2 in Table 6 when used to distinguish between AD and normal breast tissue.

Table 4: Classification results, in terms of ($A_z \pm SD$), of BEMD fractal measurements for distinguishing between AD and normal breast parenchyma

FD Features	Cross-Validation	Test
D_0	0.845 ± 0.001	0.846 ± 0.001
D_1	0.85 ± 0.006	0.849 ± 0.010
$D_1D_0^\star$	0.89 ± 0.004	0.882 ± 0.005
D_1D_2	0.903 ± 0.005	0.893 ± 0.013
$D_3D_2D_1$	0.938 ± 0.010	0.941 ± 0.009
$D_4D_3D_2D_1$	0.939 ± 0.005	0.934 ± 0.012
$D_5D_4D_3D_2D_1$	0.933 ± 0.007	0.935 ± 0.009
$D_6D_5D_4D_3D_2D_1$	0.929 ± 0.005	0.936 ± 0.009
$D_6D_5D_4D_3D_2D_1D_0^\star$	0.890 ± 0.004	0.882 ± 0.005

* the fractal dimension of the original image is included.

Table 5: Classification results, in terms of ($A_z \pm SD$), of BEMD fractal measurements for the distinguishing between surrounding tissue and AD

FD Features	Cross-Validation	Test
D_0	0.786 ± 0.001	0.777 ± 0.008
D_1	0.6 ± 0.008	0.576 ± 0.015
$D_1D_0^\star$	0.801 ± 0.006	0.793 ± 0.013
D_1D_2	0.803 ± 0.012	0.774 ± 0.019
$D_3D_2D_1$	0.856 ± 0.007	0.854 ± 0.013
$D_4D_3D_2D_1$	0.852 ± 0.007	0.851 ± 0.013
$D_5D_4D_3D_2D_1$	0.846 ± 0.009	0.837 ± 0.020
$D_6D_5D_4D_3D_2D_1$	0.834 ± 0.012	0.839 ± 0.014
$D_6D_5D_4D_3D_2D_1D_0^\star$	0.862 ± 0.007	0.869 ± 0.009

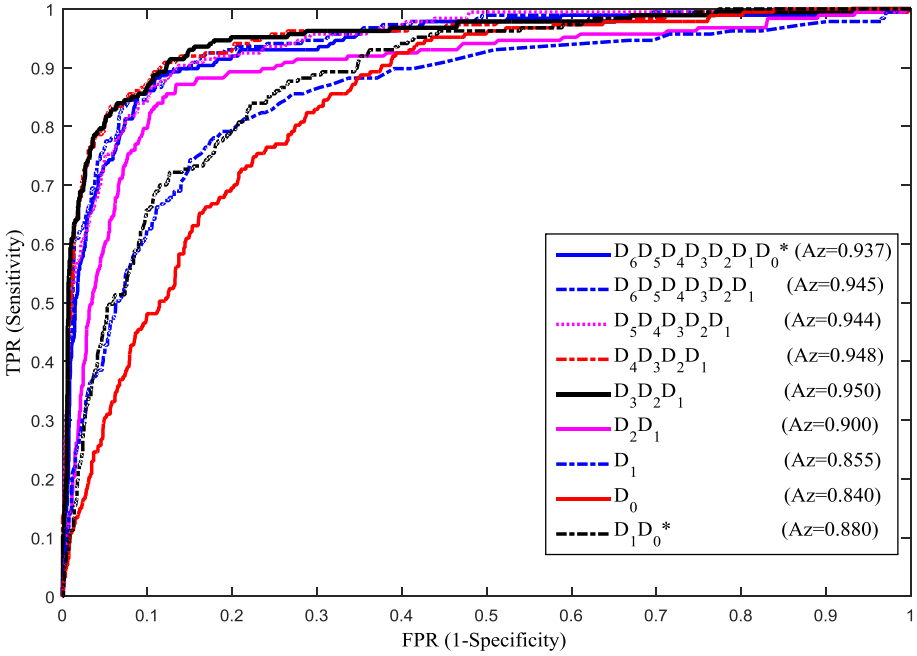

Figure 6: Best Receiver operating characteristic curves of the proposed fractal based analysis. In this illustration, the notation $D_1 \ldots D_N$ implies that fractal features were extracted from the successive and first *Nth IMF*components and $D_0^\star$ is used when the fractal dimension of the original image is included as well.

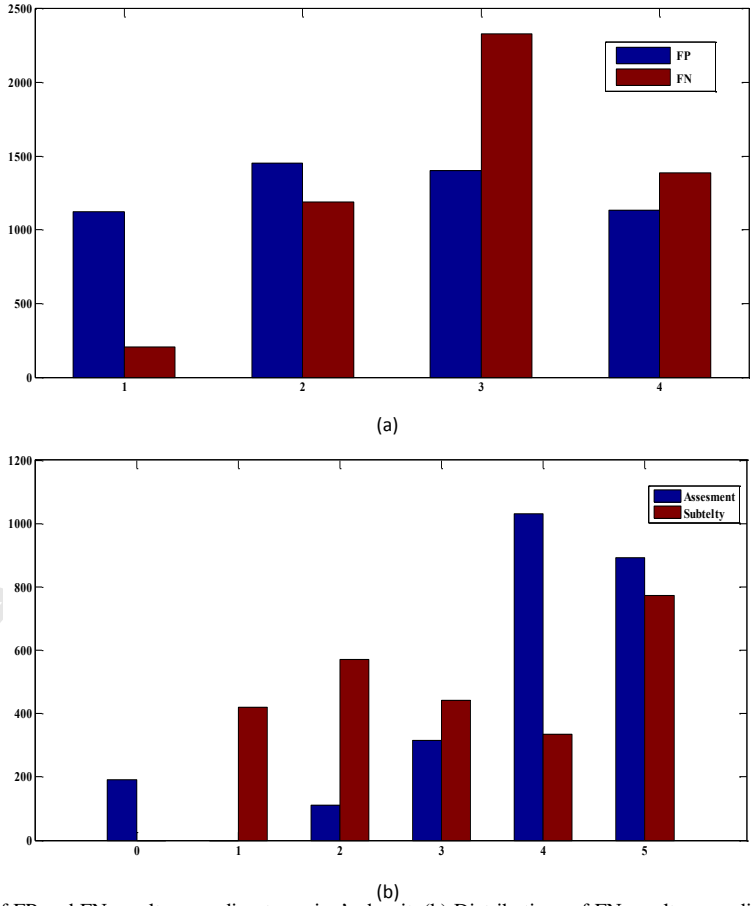

Figure 7: (a)Distributions of FP and FN results according to region's density(b) Distributions of FN results according to assessment and subtlety region ratings

Table 6: Classification results, in terms of ($A_z \pm SD$), of BEMD fractal measurements for distinguishing between normal breast parenchyma and surrounding tissue

FD Features	Cross-Validation	Test
D_0	0.572 ± 0.005	0.549 ± 0.009
D_1	0.742 ± 0.004	0.738 ± 0.003
$D_1 D_0^\star$	0.758 ± 0.006	0.745 ± 0.012
$D_2 D_1 D_2$	0.779 ± 0.004	0.771 ± 0.007
$D_3 D_2 D_1$	0.77 ± 0.007	0.761 ± 0.010
$D_4 D_3 D_2 D_1$	0.768 ± 0.006	0.762 ± 0.006
$D_5 D_4 D_3 D_2 D_1$	0.747 ± 0.004	0.748 ± 0.009
$D_6 D_5 D_4 D_3 D_2 D_1$	0.741 ± 0.004	0.738 ± 0.006
$D_6 D_5 D_4 D_3 D_2 D_1 D_0^\star$	0.78 ± 0.005	0.761 ± 0.011

4.5. Analysis of false negative and false positive results

The density of mammograms (abnormal and normal), the lesion's subtelty(or visibility) and severity are main factors influence mammographers' decision when examining screening mammography. Considering these factors we analyzed the classification results, obtained in this study, and reported, in Fig. 7(a), the distribution false positive and false negative misclassifications according to the breast density, the distribution of false negative according to the subtlety, and assessment (severity) rating of the lesion. Obtained analysis shows that the performance of multiscale fractal measurements for abnormal and normal regions were impacted by the density. That is the mammograms with higher density ratings (3 and 4) were misclassified more often, namely, regions with density rating 3. For abnormal regions classification and the false negative results associated, in addition to breast density, lesions' subtlety and severity are important factors to be considered and expected to the impact the performance of the detection task. Analysis shows that the more subtle the lesion is the higher is the risk of misclassification. For this study, in particular and as shown by in Fig. 7(b), expected abnormal regions depicting AD with highest subtlety rating 5 were misclassified more often than more visible (or less subtle) regions. However, regions with subtlety rating 2 were misclassified more frequent than region with 1 and 3 subtlety ratings. The analysis of FN results with respect to the lesion's severity has shown that regions with higher degree of severity (higher assessment rating), namely, abnormal region with assessment rating 4 were misclassified at higher frequency than other ratings.

5. Discussion and Conclusions

The underlying hypothesis of this study is that capturing the variation of fractal dimension of the intensity of a mammographic region over multiscale representation is an efficient tool for characterizing different breast tissue and, namely,for the recognizing of the architectural distortion. Previous fractal analysis [8], [10],and [9],[29] demonstrated that the fractal dimension difference between abnormal regions (architectural distortion) and normal regions is significant and that is abnormal regions show lower FD values than normal regions. However, these studies estimated a single FD measurement estimated from the original image. The fractal analysis, in this study, is multiscale and our experiments have shown, for several scales, the multiscale FD is significantly different among different classes of breast tissue: architectural distortion and its surrounding tissue, and normal breast tissue.

Unlike previous fractal based analysis [8],[10], and [9], our approach for the characterization and detection of architectural distortion, after applying BEMD algorithm to produce a multiresolution representation of the mammograhic region, extracted multiscsale FD measurements. Rather than just using a single FD value extracted from the original image, we applied multiscale fractal properties to characterize breast texture. More specifically, we exploited the variation of the fractal dimension with the change of the image resolution to characterize and discriminate textural patterns of different breast tissue (architectural distortion and its surrounding tissue, and normal breast parynchema).

For distinguishing architectural distortion from normal breast tissue, on the ROI dataset (187 AD and 2191 normal regions), described in Table 1, our fractal analysis produced $Az = 0.941 \pm 0.009$. Our results were more efficient than the performance of the parametric statistical modeling of BEMD that produced area under the receiver operating characteristic curve of 0.88. Our approach also outperformed the work in [8] that produced $Az = 0.89$ by applying the fractal dimension to distinguish 112 architectural distortion from 1388 normal regions. The fractal dimension was also previously [10] used to improve the detection of architectural distortion in suspicious mammographic regions obtained from the detection and prior mammograms reducing the number of false positive results, producing Az values of 0.68 on the detection mammogram and 0.74 on the dataset from the prior mammograms. Other studies [9] used a smaller ROI dataset (19 AD and 41 normal regions), extracted from the mini MIAS database for the evaluating the fractal based approach. For fair comparison with exiting studies [9] we have applied our approach to the MIAS dataset previously described, and achieved an average cross-validation performance of 0.964 ± 0.019. Clearly, on the MIAS dataset, our re-

sult of $Az = 0.941 \pm 0.009$ was significantly higher than Az of 0.875 obtained using fractal dimension lacunarity features in [9].

In this paper, the BEMD algorithm was used to provide a data-driven and adaptive multiresolution representation of the breast texture. The variation of fractal dimension over different scales, from BEMD, was captured and used for characterizing different types of breast texture; architectural distortion, surrounding tissue of architectural distortion, and normal breast parynchema. Consequently, the variation of the fractal dimension across different images resolutions was shown to be an efficient tool for the detection of architectural distortion textural patterns. Obtained results demonstrated that the multiscale fractal dimension not only can discriminate architectural distortion from normal breast tissue but also architectural distortion from surrounding tissue and surrounding tissue from normal breast tissue.

This study also demonstrated the ability of the proposed approach to achieve a superior and satisfactory performance in distinguishing between architectural distortion and normal breast parenchyma. Results also revealed the effectiveness of the proposed approach for the detection of architectural distortions, in digital mammogram or at least we recommend the proposed approach as a tool for reducing false positives that could be produced by an automatic detection system. Future and further extensions of this study will involve the development of an automated architectural distortion detection system, and the use of frequency information of the IMFs to characterize the speculation patterns of architectural distortions, and the extraction of other textural features such as the first and second order statistics of the IMFs.

References

[1] B. Boyer, C. Balleyguier, O. Granat, C. Pharaboz, CAD in questions/answers Review of the literature., European journal of radiology, vol.69 no.1, pp.24-33,2009.

[2] J. Tang, R. M. Rangayyan, J. Xu, I. El Naqa, Y. Yang, Computer-aided detection and diagnosis of breast cancer with mammography: recent advances, Information Technology in Biomedicine, IEEE Transactions on vol.13 no.2, pp. 236-251, 2009.

[3] R. M. Rangayyan, J. L. Desautels, S. Banik, Computer-aided detection of architectural distortion in prior mammograms of interval cancer, Synthesis Lectures on Biomedical Engineering vol.8 no.1,pp.1193,2013.

[4] A. C. of Radiology. BI-RADS Committee, A. C. of Radiology, Breast imaging reporting and data system, American College of Radiology, 1998.

[5] S. Gaur, V. Dialani, P. J. Slanetz, R. L. Eisenberg, Architectural Distortion of the Breast, 2013; 201: W662-W670. 10.2214/AJR.12.10153

[6] B. C. Yankaskas, M. J. Schell, R. E. Bird, D. A. Desrochers, Reassessment of breast cancers missed during routine screening mammography: a community-based study, American Journal of Roentgenology vol.177 no.3, pp.535-541, 2001.

[7] T. Matsubara, T. Ichikawa, T. Hara, H. Fujita, S. Kasai, T. Endo, T. Iwase, Automated detection methods for architectural distortions around skinline and within mammary gland on mammograms, in: International Congress Series, vol. 1256, Elsevier, 2003.

[8] G. D. Tourassi, D. M. Delong, C. E. Floyd Jr, A study on the computerized fractal analysis of architectural distortion in screening mammograms, Physics in medicine and biology, vol. 51 no.5, 1299,2006

[9] Q. Guo, J. Shao, V. F. Ruiz, Characterization and classification of tumor lesions using computerized fractal-based texture analysis and support vector machines in digital mammograms, International journal of computer assisted radiology and surgery vol.4, no.1, pp.11-25,2009

[10] R. M. Rangayyan, S. Prajna, F. J. Ayres, J. L. Desautels, Detection of architectural distortion in prior screening mammograms using gabor filters, phase portraits, fractal dimension, and texture analysis, International Journal of Computer Assisted Radiology and Surgery, vol.2 no.6, pp.347-361,2008.

[11] F. J. Ayres, R. M. Rangayyan, Reduction of false positives in the detection of architectural distortion in mammograms by using a geometrically constrained phase portrait model, International Journal of Computer Assisted Radiology and Surgery vol.1 no.6, pp. 361369,2007.

[12] R. Nakayama, R. Watanabe, T. Kawamura, T. Takada, K. Yamamoto, K. Takeda, Computer-aided diagnosis scheme for detection of architectural distortion on mammograms using multiresolution analysis, in: Proceedings of the 21st International Congress and Exhibition on Computer Assisted Radiology and Surgery (CARS2008), vol. 3, 2008.

[13] R. M. Rangayyan, S. Banik, J. L. Desautels, Detection of architectural distortion in prior mammograms using measures of angular dispersion, in: Medical Measurements and Applications Proceedings (MeMeA), 2012 IEEE International Symposium on, IEEE, 2012.

[14] M. M. Eltoukhy, I. Faye, B. B. Samir, Breast cancer diagnosis in digital mammogram using multiscale curvelet transform, Computerized Medical Imaging and Graphics, vol. 34 no.4 pp. 269-276,2010.

[15] N. Karssemeijer, G. M. Brake, Detection of stellate distortions in mammograms, IEEE Transactions on Medical Imaging, vol.15 no.5, pp.611619,1996

[16] M. P. Sampat, G. J. Whitman, M. K. Markey, A. C. Bovik, Evidence based detection of spiculated masses and architectural distortions, in: Proc. of SPIE Vol, vol. 5747, 2005.

[17] B. B. Mandelbrot, The fractal geometry of nature/revised and enlarged edition, New York, WH Freeman and Co., 495 p. 1,1983.

[18] H. Ahammer, Higuchi Dimension of Digital Images. PLoS ONE Vol. 6, no.9 ,e24796, doi:10.1371/journal.pone.0024796.

[19] C.-M. Wu,Y.-C. Chen, and K.-S. Hsieh, A study on the computerized fractal analysis of architectural distortion in screening mammograms, IEEE Transactions on Medical Imaging, vol.11 no.2,pp. 141–152,1992.

[20] C. B. Caldwell, S. J. Stapleton, D. W. Holdsworth, R. Jong, W. Weiser, G. Cooke, M. J. Yae, Characterization of mammographic parenchymal pattern by fractal dimension, in: 1989 Medical Imaging, International Society for Optics and Photonics, 1989.

[21] H. Ahammer, T. DeVaney, H. Tritthart, How much resolution is enough?: Influence of downscaling the pixel resolution of digi-

tal images on the generalised dimensions,Physica D: Nonlinear Phenomena vol.181 no.3, p.147-156,2003.

[22] N. E. Huang, Z. Shen, S. R. Long, M. C.Wu, H. H. Shih, Q. Zheng, N.-C. Yen, C. C. Tung, H. H. Liu, The empirical mode decomposition and the hilbert spectrum form nonlinear and non-stationary time series analysis, Proceedings of the Royal Society of London. Series A: Mathematical, Physical and Engineering Sciences vol.454 no.1971, pp.903-995,1998.

[23] J. C. Nunes, Y. Bouaoune, E. Delechelle, O. Niang, P. Bunel, Image analysis by bidimensional empirical mode decomposition, Image and vision computing, vol.21 no.12, pp.1019-1026,2003.

[24] Z. Liu, H. Wang, S. Peng, Texture classification through directional empirical mode decomposition, in: Pattern Recognition, 2004. ICPR 2004. Proceedings of the 17th International Conference on, vol. 4, IEEE, 2004.

[25] S. M. Bhuiyan, R. R. Adhami, J. F. Khan, A novel approach of fast and adaptive bidimensional emprical mode decomposition, EURASIP Journal on Advances in Signal Processing, 2008.

[26] J. C. Nunes, S. Guyot, E. Delechelle, Texture analysis based on local analysis of the bidimensional empirical mode decomposition, Machine Vision and applications, vol. 16 no.3, pp.177188, 2005.

[27] S. Sondele and I. Saini, Classification of mammograms using bidimensional empirical mode decomposition based features and artificial neural network, International Journal of Bio-Science and Bio-Technology, vol.5, no.6,pp.171–180, 2013.

[28] I. Zyout, R. Togneri, Empirical mode decomposition of digital mammograms for the statistical based characterization of architectural distortion, in: Engineering in Medicine and Biology Society (EMBC), 2015 37th Annual International Conference of the IEEE, IEEE, 2015.

[29] I. Zyout, R. Togneri, A new approach for the detection of architectural distortions using textural analysis of surrounding tissue, in: Engineering in Medicine and Biology Society (EMBC), 2016 38th Annual International Conference of the IEEE, IEEE,2015.

[30] Zhou, A. G. Podoleanu, Z. Yang, T. Yang, H. Zhao, Morphological operation based bi-dimensional empirical mode decomposition for automatic background removal of fringe patterns, Optics express, vol.20 no.22, pp.24247-24262,2012

[31] M. Heath, K. Bowyer, D. Kopans, P. Kegelmeyer Jr, R. Moore, K. Chang, S. Munishkumaran, Current status of the digital database for screening mammography, in: Digital mammography, Springer, pp. 457-460,1998.

[32] J. Suckling, J. Parker, D. Dance, S. Astley, I. Hutt, C. Boggis, I. Ricketts, E. Stamatakis, N. Cerneaz, S.-L. Kok, et al., The mammographic image analysis society digital mammogram database.

[33] Z. Liu, S. Peng, Boundary processing of bidimensional emd using texture synthesis, Signal Processing Letters, IEEE vol.12 no.1, pp.33-36, 2005.

[34] B. B. Mandelbrot, The fractal geometry of nature/revised and enlarged edition, New York, WH Freeman and Co., 495, p.1, 1983,

[35] B. Caroline, N. Vaijayanthi, Feature extraction of digital mammogram based on multidimensional complete ensemble empirical mode decomposition with adaptive noise, International Journal of Bio-Science and Bio-Technology vol.7 no.1, pp.404-409,2016.

[36] G. Rilling, P. Flandrin, P. Goncalves, et al., On empirical mode decomposition and its algorithms, in: IEEE-EURASIP workshop on nonlinear signal and image processing,vol. 3, NSIP-03, Grado (I), 2003.

[37] S. G. Mallat, A theory for multiresolution signal decomposition: the wavelet representation, IEEE Transactions on Pattern Analysis and Machine Intelligence, vol.11 no.7, pp.674-693,1989.

[38] C. Cortes, V. Vapnik, Support-vector networks, Machine learning, vlo.20 no.3, pp. 273-297,1995.

[39] C. J. Burges, A tutorial on support vector machines for pattern recognition, Data mining and knowledge discovery, Vol. 2, no.2. pp. 121-167, 1998.

[40] C.-C. Chang, C.-J. Lin, Libsvm: a library for support vector machines, ACM Transactions on Intelligent Systems and Technology. URL http://www.csie.ntu.edu.tw/ cjlin/libsvm

- Multiscale Fractal analysis of Architectural Distortion was applied
- Bidimensional EMD was applied to mammographic ROI
- Multiscale Fractal Dimension was applied
- Multiscale fractal properties of Architectural Distortions are distinct
- Results obtained are promising

.